

INESITE, HUBEITE, RUIZITE, APOPHYLLITE, AND MANGANOAN ILVAITE FROM CAVNIC, EASTERN CARPATHIANS, ROMANIA

Paulina HÎRTOBANU¹, Delia-Georgeta DUMITRAȘ², Ștefan MARINCEA²,
Nicolae CĂLIN²

¹University of Bucharest, Faculty of Geology and Geophysics, RO, paulinahirtobanu@hotmail.com

²Geological Institute of Romania, Caransebeș Str., RO-012271, Bucharest, RO, d_deliario@yahoo.com

Abstract: The rare minerals, inesite, $\text{Ca}_2\text{Mn}^{2+}_7\text{Si}_{10}\text{O}_{28}(\text{OH})_2 \cdot 5\text{H}_2\text{O}$, hubeite, $\text{Ca}_2\text{Mn}^{2+}\text{Fe}^{3+}\text{Si}_4\text{O}_{12}(\text{OH}) \cdot 2\text{H}_2\text{O}$, and ruizite, $\text{Ca}_2\text{Mn}^{3+}\text{Si}_4\text{O}_{11}(\text{OH})_4 \cdot 2\text{H}_2\text{O}$, were determined, for the first time, by optical and XRD analyses, at Căvnic (Baia Mare Neogene metallogenetic district, Eastern Carpathians, Romania) in a gold-bearing, base metal deposit. Inesite was refined as triclinic, in space group $P1$ (2), and has the following unit-cell parameters (refined from X-ray powder diffraction data): $a = 8.927(7) \text{ \AA}$, $b = 9.245(8) \text{ \AA}$, $c = 11.954(9) \text{ \AA}$; $\alpha = 91.80(2)^\circ$, $\beta = 132.60(1)^\circ$, $\gamma = 94.37(3)^\circ$, $V = 719.45(12) \text{ \AA}^3$. Hubeite was also refined as triclinic, in space group $P1$, and has as unit-cell parameters: $a = 9.960(7) \text{ \AA}$, $b = 13.870(9) \text{ \AA}$, $c = 6.562(4) \text{ \AA}$, $V = 601.19(17) \text{ \AA}^3$; $\alpha = 133.19(5)^\circ$, $\beta = 101.50(3)^\circ$, $\gamma = 66.27(4)^\circ$. Ruizite was refined on a monoclinic cell, space group $A2$ (5) and has the following unit-cell parameters: $a = 11.974(9) \text{ \AA}$, $b = 6.175(5) \text{ \AA}$, $c = 9.052(7) \text{ \AA}$, $V = 669.12(9) \text{ \AA}^3$; $\beta = 91.34(3)^\circ$. Apophyllite, $\text{KCa}_4\text{Si}_8\text{O}_{20}(\text{F},\text{OH}) \cdot 8\text{H}_2\text{O}$, is tetragonal, space group $P4/mnc$ (128), and has $a = 8.960(3) \text{ \AA}$, $c = 15.767(7) \text{ \AA}$ and $V = 1265.80(11) \text{ \AA}^3$. The terms identified represent a solid solutions series between the two end-members, fluorapophyllite and hydroxyapophyllite. Manganian ilvaite, $\text{CaFe}^{2+}\text{Fe}^{3+}(\text{Fe}^{2+}, \text{Mn})(\text{Si}_2\text{O}_7)(\text{O})(\text{OH})$, crystallizes in the space group $Pnam$ (62), and has as unit-cell parameters: $a = 13.008(7) \text{ \AA}$; $b = 8.865(5) \text{ \AA}$; $c = 5.845(3) \text{ \AA}$, $V = 674.02(9) \text{ \AA}^3$. The textural relations of inesite /hubeite/ruizite /apophyllite/manganian ilvaite assemblage show that the oldest mineral is manganian ilvaite, as inesite and hubeite overgrow and engulf this mineral. Hubeite is indicative for mildly oxidizing crystallization, conditions. Both hubeite and ruizite are Ca-Mn hydrated silicates. However, all Mn is divalent in hubeite and trivalent in ruizite. In addition, ruizite is Fe-free, whereas hubeite contains significant Fe^{3+} . Ruizite $\text{Ca}_2\text{Mn}^{3+}\text{Si}_4\text{O}_{11}(\text{OH})_4 \cdot 2\text{H}_2\text{O}$ was formed under higher oxidizing conditions as compared with hubeite. Sudoite and specularite also occurs in this oxidized assemblage. Sudoite, $\text{Mg}_2(\text{Al},\text{Fe}^{3+})_3\text{Si}_3\text{O}_{10}(\text{OH})_8$, is monoclinic and has as space group $C2m$ (12) and as unit-cell parameters $a = 5.237(2) \text{ \AA}$, $b = 9.070(5) \text{ \AA}$, $c = 14.285(8)$, $\beta = 97.0^\circ$, $V = 673.47(14) \text{ \AA}^3$. The carbonate closely associated to this assemblage is a Mn- and Ca-bearing siderite, which crystallizes in space group $R-3c$ (167), having as unit-cell parameters: $a = 4.694(1) \text{ \AA}$; $c = 15.386(5) \text{ \AA}$, and $V = 293.53(13) \text{ \AA}^3$. The secondary minerals occurring in this assemblage as determined by X-ray powder diffraction are: gold, sphalerite, pyrite, and galena. The origin of vein assemblage inesite /hubeite /ruizite /apophyllite is hydrothermal (epithermal); there exist indications of a genesis at low temperature, around 200°C . The assemblage indicated before is grown on manganian ilvaite, which is the oldest mineral in this association. There are no signs of the genesis of manganian ilvaite /inesite /hubeite /ruizite assemblage at the expense of higher T anhydrous manganese minerals such as rhodonite or johannsenite.

Keywords: inesite, hubeite, ruizite, apophyllite, manganian ilvaite, sudoite, gold, Neogene epithermal vein genesis.

1. INTRODUCTION

The Căvnic epithermal deposit is located in the eastern part of Baia Mare metallogenetic district, which belongs to the Neogene volcanic belt of East

Carpathians, Romania. The belt is characterized by the presence of many precious/base-metal hydrothermal ore deposits of low sulphidation type, like Ilba, Nistru, Săsar, Șuior, Dealul Crucii, Baia Sprie, Căvnic and Herja. The hydrothermal activity

was related to the presence of an underlying magmatic pluton of 65 km length and 15 km wide, as indicated by geophysical data. This is considered as the source of ore metals (Borcoş et al., 1975). The Cavnic deposit is a typically carbonate - base metal - gold system, with rare Au-Ag concentrations, and was intensively mined in the past. The ore deposit is of vein type and is developed on fractures trending NE-SW. Fourteen veins of 400 - 1500 m long, 1 - 8 m thick and having more than 900 m vertical development are known, hosted by Neogene volcanic rocks. In the deeper and the middle parts of the deposit the host rocks are Paleocene - Miocene sedimentary formations and dioritic bodies of Pannonian age. At the deposit scale, four main mineralization stages, that are indicative for the temperature decrease, were distinguished, as follows: (1) Fe ± W (T = 320°C); (2) Cu - Fe (T=300°C); (3) Zn - Pb - Fe - Cu (sphalerite-galena - pyrite - chalcopyrite): T= 260°C; (4) Manganese silicates and carbonates - bournonite - tetrahedrite: T = 200°C (Piantone et al., 1999). The mineralization was formed during two main time periods: 11.5 to 10.0 Ma in the western part of the district (Ilba, Nistru and Săsar), and 9.4 to 7.9 Ma in the eastern part (Herja, Baia Sprie, Şuior, and Cavnic), between 0.5 and 1.5 million years after the emplacement of the host rocks (Lang et al., 1994). The Cavnic deposit is an epithermal, low-to-intermediate sulphidation base-metal + gold type deposit (Lang et al., 1994).

The goal of this study is to describe the first Romanian occurrences of inesite, hubeite and ruizite at Cavnic, as well as to document the occurrences of apophyllite, sudoite and manganooan ilvaite.

2. SAMPLES AND ANALYTICAL METHODS

The samples analyzed were collected on the Rotunda mine dump, and belong most probably to the fourth stage, known for the crystallization of a rich paragenesis of Ca-Mn-Fe silicates and carbonates. All the Mn-Fe silicates previously mentioned by various authors are anhydrous. During this study, we determined in the Cavnic deposit inesite, hubeite, and ruizite, as first occurrences described in Romania, and apophyllite, specularite, sudoite, and manganooan ilvaite (mentioned for the first time in the Cavnic deposit). The last one is more frequently recognized as a mineral characterizing the skarn deposits (Jude, 1986; Plimer & Ashley, 1978, Bonev et al., 2005, Ilinca et al., 2006).

X-ray powder diffraction (XRD) analyses were performed using an automated Bruker (AXS)

D8 Advance diffractometer. Ni-filtered Cu K α radiation ($\lambda = 1.54056 \text{ \AA}$), a scan speed of $0.02^\circ 2\theta$ per second, a time per step of 2s, an operating voltage of 40 kV for a current of 30 mA, and a slit system of 1/0.1/1 with a receiving slit of 0.6 mm, were used for all measurements. The unit-cell parameters were calculated by least-squares refinement of the XRD data, using the computer program by Appleman & Evans (1973) modified by Benoit (1987). Synthetic silicon (NBS 640b) was used as external standard in order to verify the accuracy of measurements. The full set of X-ray powder data is available from the last author upon request.

Observations of the crystal morphologies were conducted using a MERLIN GEMINI II scanning electron microscope (SEM). Attempts to acquire energy-dispersive spectra (EDS) were made using a Tracor Northern TN-2000 system, for 100 s (live time), with an accelerating voltage of 10 kV and a beam current of 10 nA. X-ray spectra were collected and processed with the PGT semiquantitative software. Full ZAF corrections were applied to the raw X-ray data.

Optical data were acquired using a classical JENAPOL-U polarizing microscope, on both thin and polished sections.

3. THE INESITE, HUBEITE, RUIZITE, APOPHYLLITE, SUDOITE, HEMATITE, MANGANOAN SIDERITE, AND MANGANOAN ILVAITE ASSEMBLAGE

3.1. Inesite

Inesite, ideally $\text{Ca}_2\text{Mn}^{2+}_7\text{Si}_{10}\text{O}_{28}(\text{OH})_2 \cdot 5\text{H}_2\text{O}$, triclinic, occurs as prismatic crystals of a few mm long (Figure 1), and as radiating fan-shaped clusters (Figure 3). The aggregates are fibrous or massive. In transmitted light the mineral exhibits a light pink color or is colorless, having undulatory extinction. The inesite crystals have two pyroxenoid cleavages: perfect on (010) and good on (100). It is partially substituted or intergrown on the rims by hubeite crystals, which sometimes engulf inesite aggregates (Figure 2). Hubeite distinguishes itself from inesite by its higher refringence and birefringence.

In transmitted light (TL) the inesite crystals looks like they are replaced by hubeite, which is closely intergrown (Figures 1, 2, 3, 4 right, 5, and 6). Prior to this work, inesite was identified only by optical study, as new mineral for Romania, in the Cavnic deposit (Hîrtopan et al., 2012); the occurrence was now confirmed by X-ray data (Table 1).

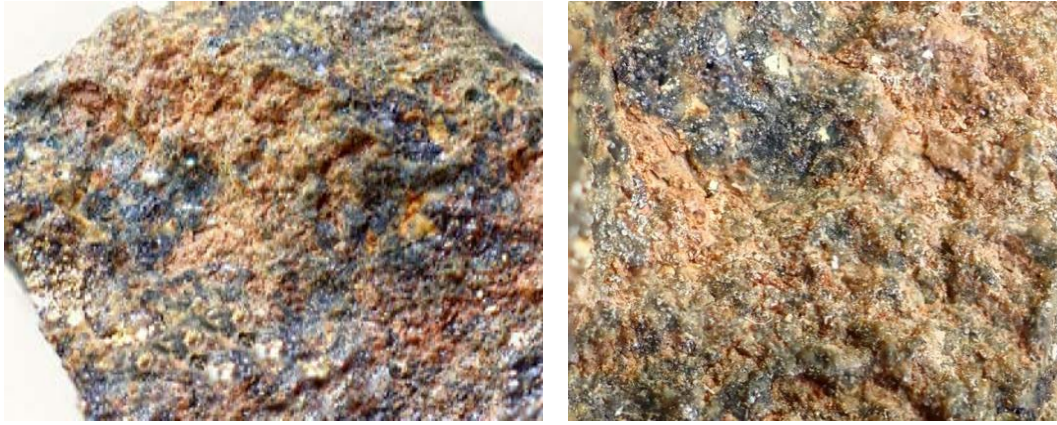


Figure 1. Inesite (pink yellow prisms) + hubeite (red brown) aggregate, manganian ilvaite (dark gray), pyrite (light yellow small grains, left bottom), and quartz (light gray) (left) in a mass of inesite + hubeite (pink red), and manganian ilvaite (gray), Cavnic specimen, x.4. Photographs by Ana Tudor.

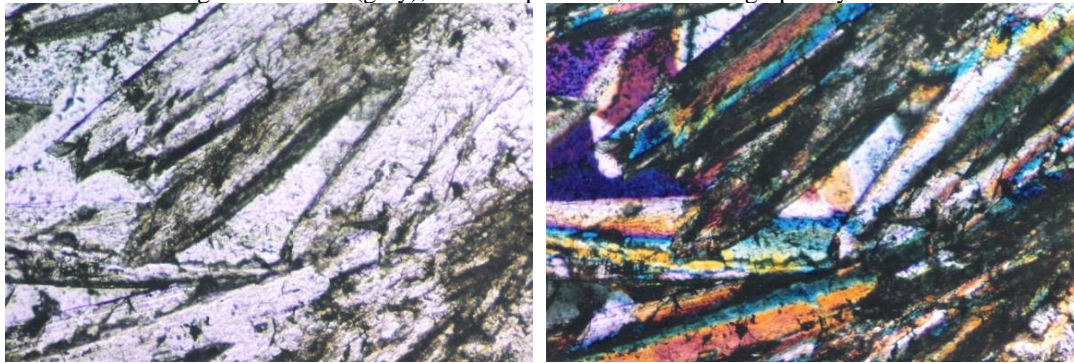


Figure 2. Inesite crystals (prisms, colorless) intergrown with hubeite (brown, needles, on the rims and inside inesite crystals), TL, NII (left) and N+ (right), x30.

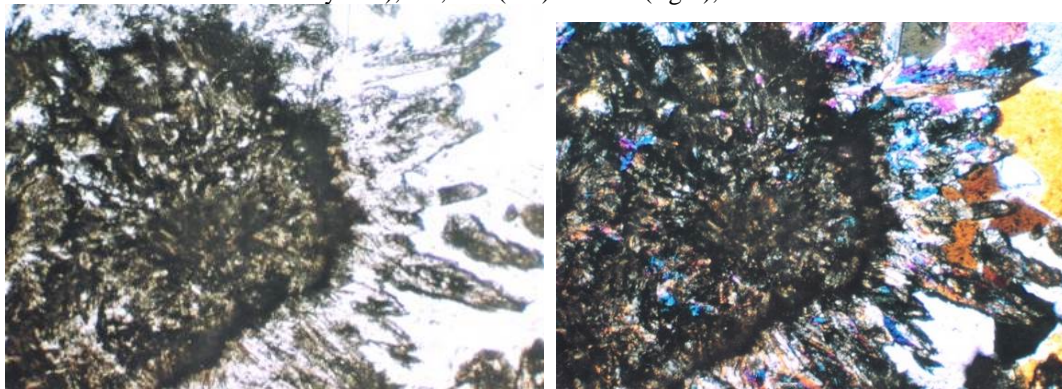


Figure 3. Radiary / stellate colorless inesite + brown hubeite crystals (right side of the picture) grown from narrow manganian ilvaite (rounded, black band, centre) and mixed small inesite + hubeite brown spherules with ilvaite black relics inside the band (left side of the picture), TL, NII (left) and N+ (right), x30.

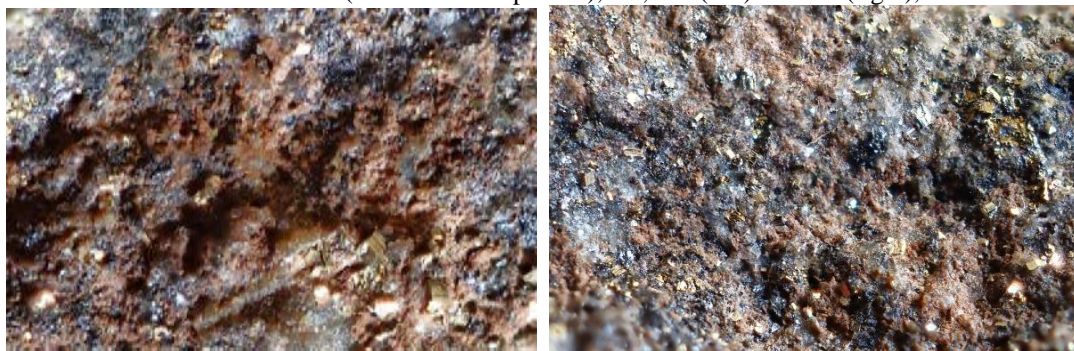


Figure 4. Clusters of hubeite (red brown to black) coated by bluish apophyllite, pyrite crystals (light yellow), and relics of manganian ilvaite (dark gray): left; hubeite (brown red), inesite (pink), apophyllite (white), quartz (light gray), and pyrite (right), Cavnic specimen, x2. Photographs by Ana Tudor.

Table 1. X-ray powder diffraction data for inesite, Cavnic

2 θ	d _{meas}	I/I ₀	(hkl)
9.648	9.160	100	(010)
13.224	6.690	10	(0.-1.1)
13.528	6.540	40	(100)
14.391	6.150	5	(-1.-1.1)
17.409	5.090	40	(-1.-1.2)
19.322	4.590	50	(020)
19.982	4.440	5	(-2.0.2)
20.258	4.380	5	(002)
20.786	4.270	30	(0.-2.1)
21.658	4.100	10	(-2.0.1)
22.150	4.010	50	(1.-2.0)
22.842	3.890	10	(-2.-1.2)
23.454	3.790	10	(-1.0.3)
24.572	3.620	10	(-1.-1.3)
25.064	3.550	10	(111)
27.335	3.260	10	(200)
27.858	3.200	10	(2.-1.0)
28.776	3.100	10	(-2.-2.2)
29.258	3.050	5	(030)
30.168	2.960	5	(-3.0.3)
30.591	2.920	80	(1.-3.0)
31.027	2.880	10	(-3.0.2)
31.475	2.840	80	(102)
32.778	2.730	70	(-3.0.4)
33.153	2.700	30	(-1.0.4)
34.062	2.630	20	(130)
35.023	2.560	30	(-3.2.3)
35.165	2.550	30	(-3.0.1)
37.604	2.390	10	(2.-3.0)
38.610	2.330	20	(-3.-2.2)
41.187	2.190	60	(-4.1.4)
41.584	2.170	40	(300)
42.402	2.130	10	(0.-4.2)
42.612	2.120	10	(1.-4.1)
44.142	2.050	10	(113)
44.370	2.040	10	(-2.2.5)
45.402	1.996	5	(-3.-3.2)
46.011	1.971	10	(-2.4.3)
46.840	1.938	10	(-4.2.5)
47.996	1.894	10	(3.-3.0)
49.269	1.848	10	(3.-1.1)
49.555	1.838	20	(0.-5.1)
51.533	1.772	10	(-1.-5.1)
51.784	1.764	5	(-4.-1.1)
53.547	1.710	10	(-5.0.6)
54.163	1.692	10	(-5.2.5)
54.512	1.682	10	(015)
55.660	1.650	30	(-1.3.5)
56.631	1.624	10	(-5.2.6)
57.363	1.605	10	(-3.5.3)
57.559	1.600	10	(-4.-2.7)
58.276	1.582	10	(-4.2.7)
58.930	1.566	10	(124)
60.242	1.535	20	(-1.2.6)
62.121	1.493	20	(-4.0.8)
62.728	1.480	20	(1.-4.4)
64.528	1.443	10	(-6.2.5)
65.289	1.428	20	(242)
66.980	1.396	10	(-5.-1.1)
68.255	1.373	20	(-4.-4.7)
70.178	1.340	10	(-2.6.4)
71.216	1.323	10	(-5.0.9)
72.545	1.302	10	(500)
74.133	1.278	10	(-2.7.2)
80.272	1.195	5	(-5.0.10)
81.757	1.177	5	(501)

The main lines in the X-ray powder diffraction pattern of inesite are given in Table 1. Based on the data in Table 1, inesite was refined as triclinic, in space group *P1* (2), and has the following unit-cell parameters (refined from X-ray powder diffraction data): $a = 8.927(7)$ Å, $b = 9.245(8)$ Å, $c = 11.954(9)$ Å; $\alpha = 91.80(2)^\circ$, $\beta = 132.60(1)^\circ$, $\gamma = 94.37(3)^\circ$, $V = 719.45(12)$ Å³. Inesite is closely associated with hubeite (Figures. 1, 2, 3, 4 right, 5, and 6). The intimate physical association of hubeite and inesite in the Cavnic deposit is due to the close structural affinity, density, and H₂O contents of these minerals (Cooper & Howthrow, 2004). The association itself belongs to a late hydrothermal (epithermal) stage of the manganoan ilvaite – (inesite + hubeite) – (ruizite + apophyllite) sequence in the deposit.

The rhodonite presence in other places of the deposit is indicative for an earlier, prograde and higher T stage. In fact, the Mn- and Fe-rich inesite + hubeite + ruizite + manganoan ilvaite assemblage from Cavnic must probably originate from a Mn-bearing skarn. However, the actual look of the inesite + hubeite + ruizite + manganoan ilvaite assemblage is that of a typical hydrothermal-epithermal vein, with no relics of Mn-anhydrous pyroxene and/or Mn-pyroxenoids. The fluid inclusion study (Piantone et al., 1999) revealed a global cooling of the Cavnic ore system from 320°C (stage 1) to 200°C (stage 4, containing Mn silicates + tetrahedrite + bournonite + carbonates). Temperature of stage 4 is too low for the crystallization and stability of hydrothermal rhodonite, which needs a

temperature higher than 400°C (Momoi, 1974). Therefore, all the hydrous Mn-Fe silicates of this stage are of lower T than the rhodonite formation.

3.2. Hubeite,

Ideally $\text{Ca}_2\text{Mn}^{2+}\text{Fe}^{3+}\text{Si}_4\text{O}_{12}(\text{OH})\cdot 2\text{H}_2\text{O}$, hubeite was mentioned for the first time in a Romanian occurrence. The mineral is named from the Hubei province in China, in which it was found as new mineral. Hubeite was approved by the Commission of New Minerals and Mineral Names of the International Mineralogical Association in 2002. It shows no close relationships to any other mineral, excepting inesite. In the Cavnic deposit it was determined optically, in transmitted light, and was confirmed by X-ray powder diffraction. The mineral occurs as millimeter-sized radiating aggregates of crystals closely associated with inesite (Figures 1, 2, 3, 4 right, 5, and 6), with apophyllite + quartz + pyrite (Figure 4, right), with inesite+ apophyllite + pyrite + quartz (Figure 4 right), and with manganooan ilvaite (Figures 12 and 13). The hubeite aggregates frequently form divergent fan-like clusters (Figures 3, 6, 7) and bow-tie arrangements (Figure 6). Under the microscope, the individual crystals show a strong pleochroism, from brown, light brown to yellow and dark brown, and presents a good cleavage on (001). Hubeite differs from inesite by its strong pleochroism and slightly lower refringence. The strongest lines in the X-ray powder diffraction pattern are depicted in Table 2. Hubeite is triclinic, space group *P*1. Its unit-cell parameters, refined by least squares from X-ray powder-diffraction data in Table 2 are: $a = 9.960(7)$ Å, $b = 13.870(9)$ Å, $c = 6.562(4)$ Å, $V = 601.19(17)$ Å³; $\alpha = 133.19(5)^\circ$, $\beta = 101.50(3)^\circ$, $\gamma = 66.27(4)^\circ$. These values are very close to that of hubeite from the type locality in Hubei Province, China (Howthorne, et al., 2002). The structure of hubeite is heteropolyhedral with alternating layers of tetrahedrons and different polyhedrons parallel to (001). Both hubeite and inesite are minerals with a structure based on layers of edge-sharing (Ca-Mn-Fe) polyhedrons that alternate with layers of Si tetrahedrons (Howthorne et al., 2002). In the Cavnic deposit, hubeite is closely associated with inesite and contain relics of manganooan ilvaite. The reciprocal textural relationships show that the inesite and hubeite are grown on manganooan ilvaite (Figure 2). The Fe^{3+} in hubeite comes most probably from manganooan ilvaite. The conditions during the crystallization of hubeite were mildly oxidizing (Howthorne et al., 2002).

The second known worldwide occurrence of hubeite is a specimen reported in the old museum of

the Harstigen mine, Sweden. It occurs in a pyroxene skarn, being associated with rhodonite, barite, gonyerite and calcite (Holtstam, 2020). The Cavnic hubeite defines therefore the third occurrence of this mineral in the world. Hubeite from Cavnic seems to be formed on the expense of manganooan ilvaite, which most probable has a hydrothermal origin. Hubeite is closely associated with inesite (Figures 3 and 4) and apophyllite (Figure 5), and does not include rhodonite and/or johannsenite relics.

3.3. Ruizite

Ruizite ideally $\text{Ca}_2\text{Mn}^{3+}\text{Si}_4\text{O}_{11}(\text{OH})_4\cdot 2\text{H}_2\text{O}$, is a sorosilicate mineral, with structure based on $[\text{Si}_4\text{O}_{11}(\text{OH})_2]$ linear clusters of corner-sharing tetrahedrons, like in the hubeite structure. This is the first purely silicate clusters of this type to be found in a mineral structure (Howthorne, 1984; Moore et al., 1985). The last refinement of the ruizite crystal structure (Fendrich et al., 2016), shows that it consists of [010] chains of edge-sharing MnO_6 octahedrons flanked by finite $[(\text{Si}_4\text{O}_{11})(\text{OH})_2]$ chains. The seven-fold coordinated Ca^{2+} cations are situated in the cavities of this arrangement. Ruizite from Cavnic occurs as long prismatic or acicular crystals of about a few mm long. In transmitted light the mineral has yellow orange to brown and dark brown color (Figures 8 left and right, and Figures 9 left and right). It has medium refringence, high birefringence (Figure 6, right), and is biaxial negative. Both hubeite and ruizite are Ca-Mn hydrated silicates. However, all Mn is divalent in hubeite and trivalent in ruizite. In addition, ruizite is Fe-free, whereas hubeite contains significant Fe^{3+} and does not contain Mn^{3+} , which implies that ruizite was formed under higher oxidizing conditions than hubeite. At Cavnic, ruizite associates with apophyllite (Figures 8), manganooan ilvaite (Figure 9 left), specularite, sudoite, quartz, siderite (Figure 9 right) and sphalerite.

Ruizite, as new mineral species, has been approved by the Commission of New Minerals and Mineral Names of the International Mineralogical Association in 1977. It was determined for the first time in Christmas copper mine, Arizona (Williams & Duggan, 1977). The second occurrence of ruizite was reported in the Wessels mine, South Africa (Wilson & Dunn, 1978). Ruizite was found also in Cornwall mine, Lebanon County, Pennsylvania (Kearns & Kearns, 2008), and in the Cerchiara mine, Liguria (Balestra et al., 2009). The discovery of ruizite at Cavnic raises to fifth the worldwide occurrences of this mineral.

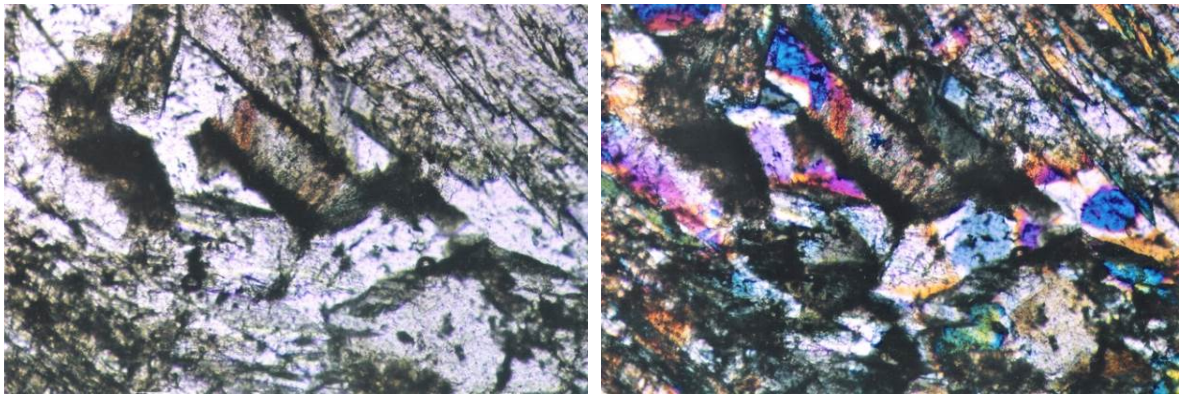


Figure 5. Inesite (white prisms, center) intergrown with hubeite (needles, light brown, top right and bottom left corners), ruizite (small, orange, in center), and manganoan ilvaite relics (black). TL, N II (left) and N+ (right), x35.

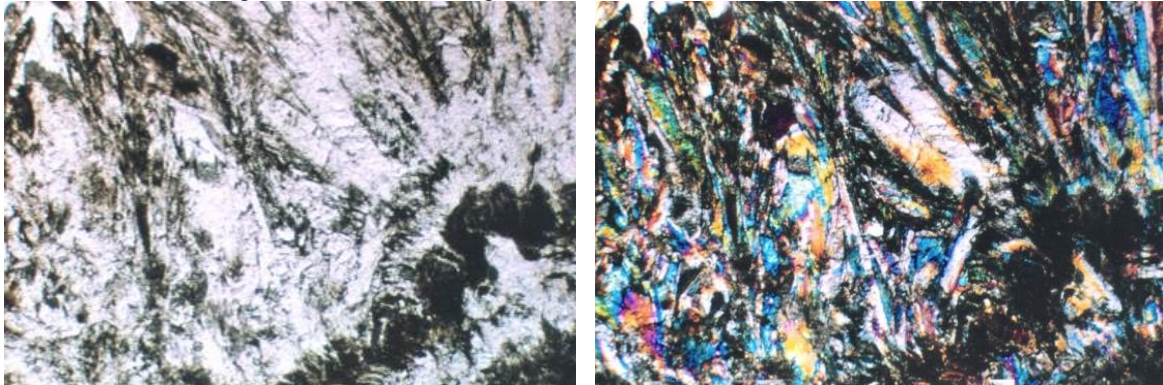


Figure 6. Hubeite (large acicular crystals, light brown, with "bow tie" arrangement), intergrowth with inesite (large white prisms), manganoan ilvaite (brown black rounded band in the right bottom corner) from which grow small fan-shaped inesite aggregates intergrown with hubeite. TL, NII (left) and N+ (right), x35.

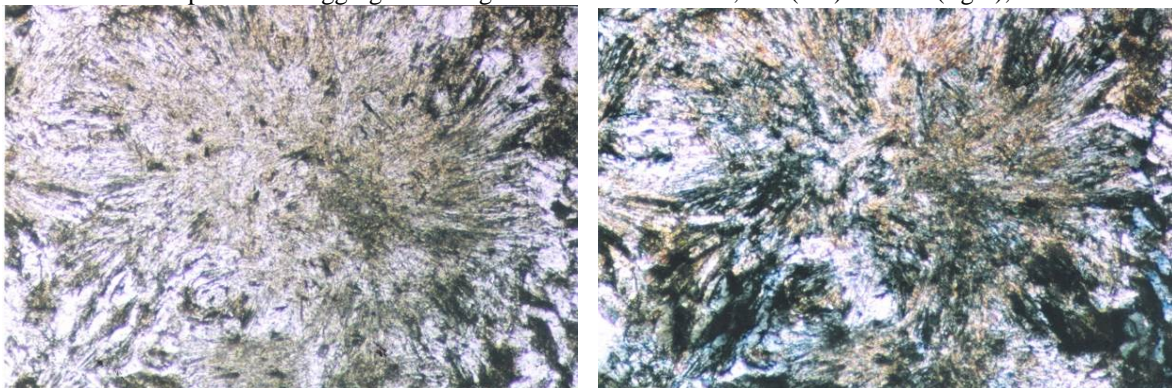


Figure 7. Hubeite fan-like or radiating clusters (brown - light brown - yellow, acicular) associated with apophyllite (white, small, low birefringence). TL, NII (left) and N+ (right), x35.

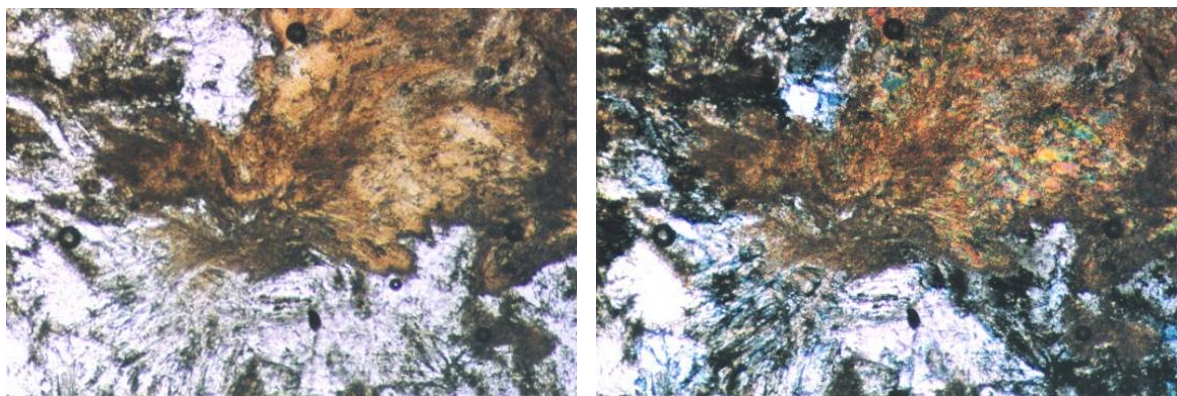


Figure 8. Ruizite (brown, light brown, high birefringence), apophyllite (white gray, good cleavages, and low birefringence), and quartz (white), TL, N II (left) and N+ (right), x35.

Table 2. X-ray powder diffraction data for hubeite, Cavnic

2 θ	d _{meas.}	I/I ₀	(hkl)	2 θ	d _{meas.}	I/I ₀	(hkl)
9.742	9.072	100	(100)	34.995	2.562	3	(221)
10.731	8.238	90	(110)	35.862	2.502	5	(240)
15.151	5.843	10	(0.-2.1)	35.862	2.502	5	(0.-5.2)
15.151	5.843	10	(-1.-2.1)	36.496	2.460	3	(2.-2.2)
15.881	5.576	5	(-1.1.0)	37.818	2.377	5	(002)
16.482	5.374	5	(-1.-1.1)	39.366	2.287	5	(321)
17.725	5.000	30	(120)	41.069	2.196	3	(-3.2.0)
18.217	4.866	3	(210)	41.705	2.164	20	(-1.-5.3)
18.773	4.723	10	(020)	42.697	2.116	5	(231)
18.773	4.723	10	(001)	42.697	2.116	5	(-2.-5.3)
19.973	4.442	20	(101)	43.298	2.088	3	(0.-5.3)
22.133	4.013	20	(-1.0.1)	44.007	2.056	10	(-1.-6.1)
23.053	3.855	5	(-2.-1.1)	44.810	2.021	20	(-2.2.1)
24.333	3.655	10	(-1.2.0)	45.474	1.993	30	(331)
24.844	3.581	10	(-2.1.0)	47.411	1.916	15	(510)
25.311	3.516	3	(2.-1.1)	47.835	1.900	3	(1.-6.2)
25.780	3.453	3	(111)	50.138	1.818	15	(-4.-7.2)
26.166	3.403	15	(011)	51.161	1.784	3	(2.-2.3)
27.929	3.192	30	(230)	51.161	1.784	3	(-5.-1.1)
28.531	3.126	70	(320)	51.816	1.763	3	(511)
28.823	3.095	70	(-1.-4.2)	51.816	1.763	3	(0.-1.3)
29.848	2.991	10	(-1.1.1)	52.326	1.747	3	(-3.2.1)
30.463	2.932	25	(0.-4.2)	53.045	1.725	3	(-4.-4.3)
30.463	2.932	25	(-2.-3.2)	54.129	1.693	3	(-2.3.1)
31.060	2.877	15	(1.-2.2)	54.129	1.693	3	(5.-1.1)
32.161	2.781	60	(-2.2.0)	55.260	1.661	3	(-5.-7.2)
32.643	2.741	15	(3.3.0)	55.733	1.648	5	(160)
33.216	2.695	30	(-1.-5.2)	55.733	1.648	5	(3.-5.2)
33.771	2.652	3	(-1.-1.2)	56.517	1.627	30	(1.-7.3)
33.832	2.614	10	(2.-3.1)	56.517	1.627	30	(-1.-5.4)

3.4. Apophyllite

Apophyllite, ideally $\text{KCa}_4\text{Si}_8\text{O}_{20}(\text{F},\text{OH})\cdot 8\text{H}_2\text{O}$, belongs to a solid solutions series between fluorapophyllite [apophyllite-(KF)] and hydroxyapophyllite [apophyllite-(KOH)]. The X-ray powder data established for the Cavnic apophyllite (available under request from the last author) show that the mineral is tetragonal, space group $P4/mnc$ (128), and has $a = 8.960(3)$ Å, $c = 15.767(7)$ Å and $V = 1265.80(11)$ Å³. The pattern is indicative for a fluorapophyllite, as it contains numerous minimum intensity reflections which are not observed at hydroxyapophyllite. The cell dimensions of fluorapophyllite, as well as the cell volume, are slightly smaller than those of hydroxyapophyllite (Colville et al., 1971). As the Cavnic apophyllite has cell dimensions smaller than those of hydroxyapophyllite, we suppose that it represents a term close to the fluorapophyllite end-member.

In transmitted light apophyllite occurs as tabular, colorless to pale yellow, pale pink or pale

green crystals. The mineral has low refringence and birefringence (Figure 10). Optically is uniaxial positive. The Cavnic apophyllite is associated with hubeite (Figure 4), ruizite and manganian ilvaite (Figures 8 and 9 left).

3.5. Sudoite

Sudoite, ideally $\text{Mg}_2(\text{Al},\text{Fe}^{3+})_3\text{Si}_3\text{O}_{10}(\text{OH})_8$, belongs to the chlorite group, having a rare dioctahedral structure. In transmitted light it has light green to colorless tints. The mineral occurs as mica-like grains and has low refringence and birefringence.

The main lines in the X-ray powder diffraction pattern, expressed in terms of inter-reticular distances (in Å), relative intensity I/I_0 (%), and Miller indices (hkl) are given in Table 4. Based on the X-ray powder data in Table 4, the mineral was refined as monoclinic, in space group $C2m$ (12) and has as unit-cell parameters: $a = 5.237(2)$ Å, $b = 9.070(5)$ Å, $c = 14.285(8)$, $\beta = 97.0^\circ$, $V = 673.47(14)$ Å³.

Sudoite associates with apophyllite (Figure 9), hematite (Figure 9, right), and manganian ilvaite

Table 3. X-ray powder diffraction data for ruizite, Cavnic

2 θ	d _{meas}	I/I ₀	(hkl)	2 θ	d _{meas}	I/I ₀	(hkl)
7.361	12.000	100	(100)	36.728	2.44500	10	(213)
14.827	5.970	10	(200)	37.572	2.39200	5	(500)
17.409	5.090	50	(011)	38.593	2.33100	30	(222)
18.866	4.700	10	(-1.1.1)	40.836	2.20800	5	(104)
19.668	4.510	30	(002)	41.484	2.17500	5	(-5.1.1)
21.187	4.190	70	(102)	41.907	2.15400	5	(511)
22.319	3.980	30	(300)	42.361	2.13200	40	(322)
23.083	3.850	10	(211)	43.211	2.09200	10	(502)
24.435	3.640	40	(-2.0.2)	44.670	2.02700	10	(-4.1.3)
24.993	3.560	10	(202)	45.741	1.98200	30	(413)
28.587	3.120	60	(311)	47.098	1.92800	5	(422)
28.967	3.080	10	(020)	47.543	1.91100	5	(-2.3.1)
29.899	2.986	10	(400)	48.077	1.89100	10	(520)
30.262	2.951	40	(302)	48.707	1.86800	5	(-6.1.1)
32.655	2.740	30	(220)	49.991	1.82300	10	(-4.0.4)
33.103	2.704	10	(013)	51.223	1.78200	20	(404)
33.810	2.649	30	(-1.1.3)	52.070	1.75500	20	(-5.2.2)
34.142	2.624	20	(113)	52.716	1.73500	20	(224)
34.591	2.591	40	(-4.1.1)	53.615	1.70800	20	(115)
35.208	2.547	30	(022)	54.794	1.67400	20	(-2.1.5)
35.612	2.519	40	(-4.0.2)	55.807	1.64600	50	(324)
36.101	2.486	20	(122)				

Table 4. X-ray powder diffraction data for sudoite, Cavnic

2 θ	d _{meas.}	I/I ₀	(hkl)	2 θ	d _{meas.}	I/I ₀	(hkl)
6.219	14.200	80	(001)	44.740	2.024	6	(007)
12.404	7.130	70	(002)	45.692	1.984	50	(204)
18.705	4.740	80	(003)	48.707	1.868	16	(135)
19.625	4.520	85	(110)	50.315	1.812	25	(205)
20.591	4.310	6	(021)	53.547	1.710	16	(240)
21.239	4.180	6	(111)	55.918	1.643	6	(-2.4.3)
22.094	4.020	6	(-1.1.2)	59.346	1.556	40	(137)
23.144	3.840	2	(022)	61.300	1.511	60	(207)
25.064	3.550	65	(004)	62.823	1.478	10	(-3.3.3)
27.250	3.270	2	(023)	64.729	1.439	6	(-3.3.4)
28.967	3.080	4	(113)	65.808	1.418	2	(0.0.10)
30.559	2.923	2	(-1.1.4)	67.362	1.389	40	(315)
31.487	2.839	20	(005)	70.724	1.331	2	(-3.3.6)
32.137	2.783	2	(024)	72.870	1.297	16	(-2.6.2)
34.385	2.606	10	(200)	74.405	1.274	18	(335)
35.251	2.544	25	(131)	75.656	1.256	10	(-4.2.2)
35.877	2.501	100	(-1.3.2)	78.536	1.217	10	(403)
37.297	2.409	50	(132)	81.339	1.182	2	(0.0.12)
38.303	2.348	25	(-1.3.3)	82.957	1.163	2	(-1.7.5)
40.416	2.230	25	(133)	86.045	1.129	2	(1.3.11)
41.786	2.160	2	(042)				

(Figure 13). The hydrothermal origin of this mineral was already accepted (e.g., Eggleston & Bailey,

1967). The crystallization of sudoite occurs under relatively higher T and from highly supersaturated

fluids as compared with many other hydrothermal clay minerals described so far (Jige et al., 2018). The Al-rich clay minerals such as sudoite, tosudite, rectorite, crystallize at 270 - 200°C in the hydrothermal system, whereas sudoite forms at slightly higher T than tosudite and rectorite (Jige et al., 2018).

3.6. Manganooan calcian siderite

This carbonate is directly associated with the manganooan ilvaite + inesite + hubeite + apophyllite + ruizite assemblage. It has a complex composition with high Fe > Mn > Ca, and lower Ba and Mg contents. Its electron diffraction spectrum can be seen in Figure 11. In Figure 9 right, the textural relations show that the manganooan calcian siderite is older than ruizite and the crystallization of manganooan ilvaite precludes that of ruizite. The crystallization sequence is: manganooan ilvaite – manganooan calcian siderite - ruizite. The main lines in the X-ray powder diffraction pattern, expressed in terms of d spacings (in Å), relative intensities (I/I₀ %) and Miller indices (hkl) are: 3.593, 25, (012); 2.795, 100, (104); 2.346, 20, (110); 2.134, 20, (113); 1.965, 20, (202); 1.7382, 30, (018); 1.7315, 35, (116). The mineral could be satisfactorily refined in space group R-3c (167), having as unit-cell parameters: *a* = 4.694(1) Å; *c* = 15.386(5) Å, and *V* = 293.53(13) Å³. Siderite associates with manganooan ilvaite, hematite and sudoite, in the epithermal metallic veins of the Cavnic deposit.

3.7. Manganooan ilvaite

Ideally CaFe²⁺Fe³⁺(Fe²⁺,Mn)(Si₂O₇)(O)(OH), manganooan ilvaite occurs as randomly oriented large prismatic crystals of a few mm until 1cm in length, inducing a banded to compact texture of the ore (Figures 12 and 13).

It is translucent, with iron black, dark grayish to black brittle color, and has submetallic luster (Figures 12 and 13 with distinct (001) and (010) cleavages).

In transmitted light the mineral is transparent and has an intense pleochroism: X = dark green, Y = yellow, red, and brown to dark brown and Z = dark brown to black (Figure 14). In reflected light, the pleochroism is from light gray to bluish gray, pinkish red to violet. The mineral is strongly anisotropic, with red internal reflections. The back scattered electron images shows that the mineral is homogeneous (Figure 15 left), having no major compositional variations. The simplified electron diffraction spectrum of Cavnic manganooan ilvaite

can be seen in Figure 15 right, whereas the chemical composition is given in Table 5.

Table 5. Chemical composition of manganooan ilvaite,

Oxyde	wt.%	cations (p.f.u.) ⁽¹⁾
SiO ₂	31.313	6.0502
TiO ₂	0.047	0.0068
Al ₂ O ₃	0.130	0.0295
FeO ⁽²⁾	49.956	8.0726
MnO	4.917	0.8048
MgO	0.182	0.0525
CaO	14.064	2.9118
Na ₂ O	0.000	0.0000
K ₂ O	0.001	0.0001
Cl	0.004	0.0013
Cl = O	-0.001	-
Total	100.612	17.9295

Cavnic*

* as obtained by electron microprobe analysis; (1) as calculated on a basis of 24 oxygen anions in the anhydrous part of formula; (2) all iron as FeO

The main lines in the X-ray powder diffraction pattern of a selected sample of manganooan ilvaite expressed in terms of d spacings (in Å), relative intensities (I/I₀, %) and Miller indices (hkl) are: 7.2961, 84, (110); 6.507, 29, (200); 3.895, 23, (310); 3.252, 24, (400); 3.241, 20, (311); 2.882, 38, (130); 2.845, 97, (401); 2.845, 97, (4.0.-1); 2.715, 100, (112); 2.715, 100, (1.1.-2); 2.706, 57, (411); 2.690, 67, (230); 2.677, 72, (230); 42.444, 36, (330); 2.435, 46, (231); 2.435, 46, (2.3.-1); 2.388, 29, (421); 2.388, 29, (4.2.-1); 2.174, 28, (402); 2.113, 41, (412); 2.113, 41, (4.1.-2); 2.106, 26, (610); 1.898, 24, (512); 1.498, 26, (632); 1.498, 26, (6.3.-2); 1.471, 44, (252); 1.471, 44, (2.5.-2); 1.463, 28, (004). Based on these data, the mineral could be satisfactorily refined in space group *P*2₁/*b*, and has as unit-cell parameters: *a* = 13.008(7) Å; *b* = 8.865(5) Å; *c* = 5.845(3) Å, *β* = 90.12(1)°, *V* = 674.02(9) Å³. The values before are reasonably close by those reported by Bonev et al., (2005) for manganilvaite from Rhodope (*a* = 13.025 Å; *b* = 8.8514 Å; *c* = 5.8486 Å, *β* = 90.167°) or by Ilinca et al., (2006) for the manganilvaite from Dognecea (*a* = 13.014 Å, *b* = 8.846 Å, *c* = 5.848 Å, and *β* = 90.34°).

Manganooan ilvaite from Cavnic has no relics of early-skarn pyroxenes (hedenbergite - johannsenite) and pyroxenoids (rhodonite and bustamite), such as Rhodope (Bonev et al., 2005) and Dognecea (Ilinca et al., 2006) Mn-bearing ilvaite, respectively, which suggests that the mineral is not a retrograde alteration product, but a vein mineral, issued from a hydrothermal process, as well as the inesite + hubeite + ruizite assemblage. According to Ilinca et al., (2006), the Dognecea manganilvaite is formed at temperatures up to 300°C,

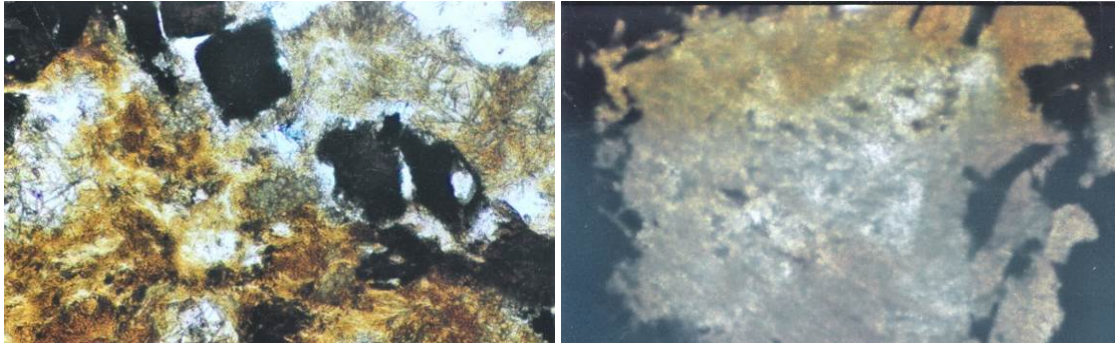


Figure 9. Ruizite (yellow, brown), manganian ilvaite (black), apophyllite (white, good cleavage), sphalerite (small, gray, center), and quartz (white): left; ruizite (yellow, orange) with manganian ilvaite relics (black), siderite (gray, center), sudoite (gray greenish), and quartz (white) (right), TL, N II (left) and N+ (right), x40.

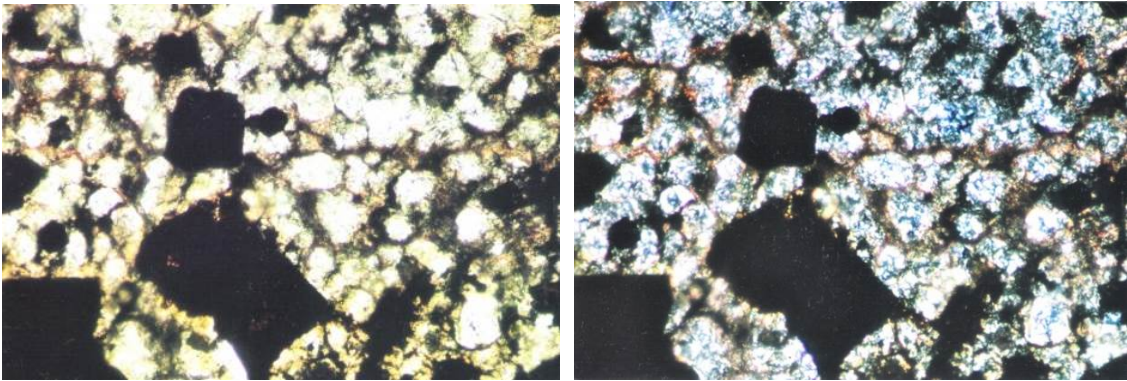


Figure 10. Apophyllite (white, isometric, low birefringence), replacing manganian ilvaite. Sudoite (green - light green), surrounds apophyllite grains. Transmitted light, N II (left) and N+ (right), x35.

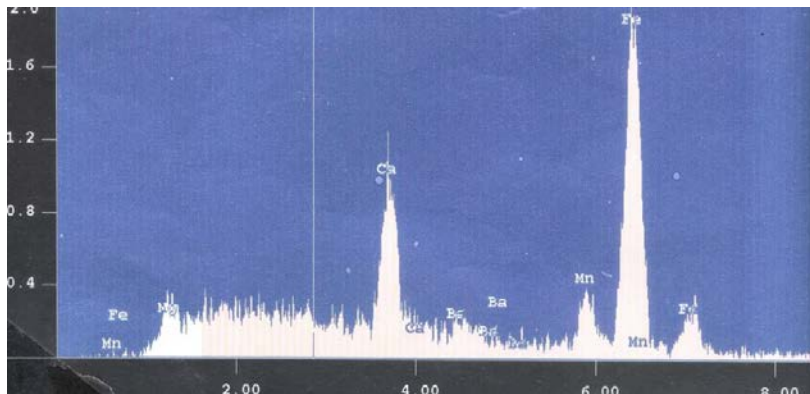
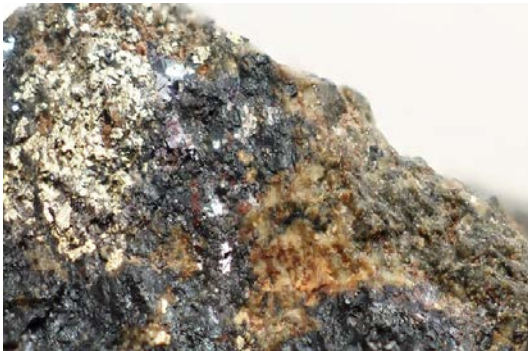


Figure 11. Simplified electron diffraction spectrum of manganian calcian siderite.



Figures. 12 (left) and 13 (right). Fig. 12. Manganian ilvaite (gray) cut by hubeite vein (red brown) + quartz (white, left) and pyrite (white yellow, top left), x2. Fig. 13. Manganian ilvaite (gray dark black), inesite + hubeite (pink, red, yellow), ruizite (red, around manganian ilvaite relics: top), quartz (white-gray), and sudoite (green), x4. Cavnic specimens. Photographs by Ana Tudor.

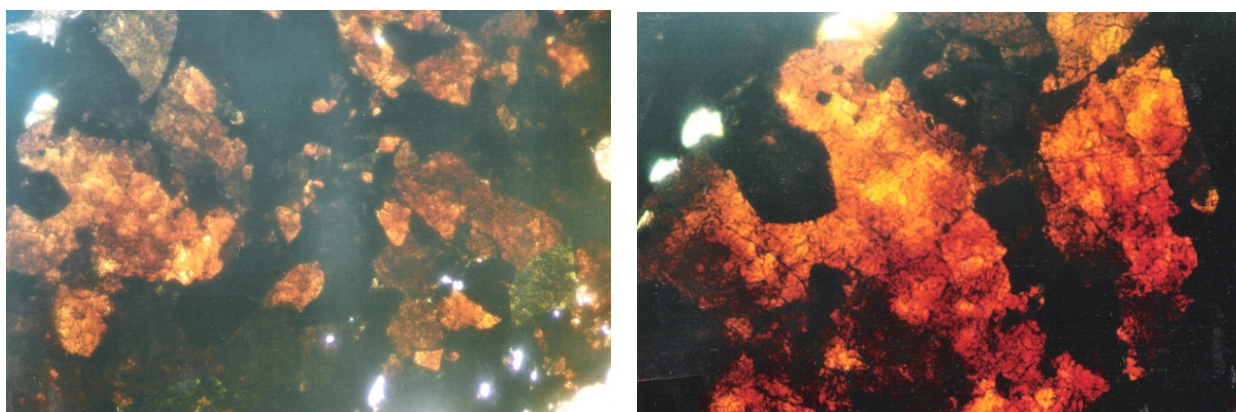


Figure 14. Manganoan ilvaite with high pleochroism: yellow – red-brown – green, and black (left and right). TL, N II (left) and N+ (right), x30.

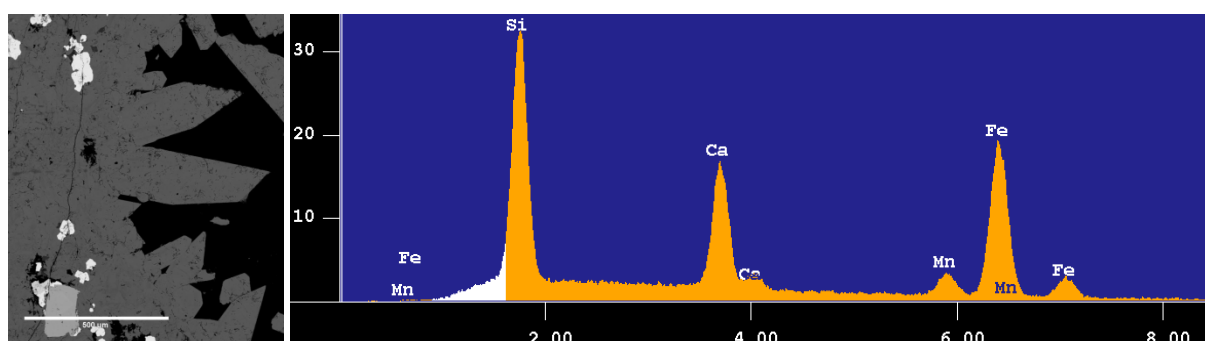


Figure 15. Backscattered electron image of manganoan ilvaite (large gray crystals), native gold (white small grains) on the veins, pyrite (light gray), and quartz (black) in the left side of the photograph, and its electron diffraction spectrum (right). (Hirtopanu et al., 2012)

in relatively of low fO_2 conditions (Ilinca et al., 2006). In our opinion, the manganoan ilvaite from Cavnic forms at higher temperatures and oxygen fugacities, in a hydrous environment, the mineral being the oldest mineral of the hydrothermal assemblage. Manganoan ilvaite was also mentioned in Ghezuri deposit of the Oaş Neogene metallogenic district, in a high temperature, pneumatolitic, paragenesis, associated with magnetite, pyrrhotite, chalcopyrite, cubanite, pyrite, and native gold (Jude, 1986). Manganilvaite, first described as new mineral species by (Bonev et al., 2005) in deposits from Rhodope, was identified in the skarns from Dognecea (southwestern Banat) by Ilinca et al., (2006), associated with Mn-hedenbergite and magnetite. The skarn ilvaite is generally much richer in Mn (varying from 8.60 wt.% MnO to 15.03 wt.% MnO) than ilvaite from the hydrothermal veins (Larsen & Dahlgren 2002). The manganoan ilvaite from Broken Hill, New South Wales, and Ban Ban, Queensland, Australia contains up to 13.5 wt.% MnO, and 12.42 wt.% MnO, respectively (Bonev et al., 2005). Manganoan ilvaite from Broken Hill was formed as an early retrograde metamorphic phase from calcic rhodonite, in the polymetamorphosed Pb-Zn sulfide/manganese silicate rocks at Broken-Hill, whereas ilvaite from Ban Ban was formed as at the

expense of pyroxene, in the grossular-andradite skarn (Plimer & Ashley, 1978). The content of MnO of the Cavnic manganoan ilvaite, as determined by electron microprobe (4.917 wt.%) was also estimated based on the electron diffraction spectrum in Figure 13 (right), as of about 5 wt.%, enough to define a manganoan ilvaite, with more than 25% of the structural sites normally occupied by Fe^{2+} filled by Mn^{2+} . For comparison, the MnO content of the Rhodope manganilvaite varies in the range of 9.02 - 14.96 wt.% (Bonev et al., 2005), and that of Dognecea manganilvaite in the range of 7.30 - 9.17wt% (Ilinca et al., 2006).

3.8. Hematite

Hematite, $\alpha-Fe_2O_3$, occurs in Cavnic deposit as the specularite variety. The mineral occurs as acicular radiating aggregates and mica-like rosettes. In reflected light the bireflectance colors are white and gray white with bluish tint. The blood red internal reflections are visible in all cases. Optically the mineral is uniaxial negative. Specularite closely associates with sudoite, siderite, manganoan ilvaite and ruizite.

The main lines in the powder diffraction pattern, expressed in terms of d spacings (in Å),

relative intensities (I/I_0 , %) and Miller indices (hkl) are: 3.682, 30, (012); 2.700, 100, (104); 2.518, 72, (110); 2.207, 19, (113); 1.8412, 35, (024); 1.6947, 43, (116); 1.4862, 28, (214); 1.4536, 27, (300); 1.1409, 7, (134). The mineral could be satisfactorily refined in space group $R\bar{3}c$ (167), having as unit-cell parameters: $a = 5.035(3)$ Å; $c = 13.749(5)$ Å; $V = 301.9(9)$ Å³.

3.9. Rhodonite

Rhodonite, ideally $MnSiO_3$, is associated with calcite and quartz (Figure 15) belonging most

probable to an early stage of crystallization, preceding the formation of hubeite. The main lines in the powder diffraction pattern, expressed in terms of d spacings (in Å), relative intensities (I/I_0 , %) and Miller indices (hkl) are: 3.340, 25, (002); 3.140, (30), (221); 3.100, 25, (210); 2.980, (65), (112); 2.924, 65, (130); 2.772, 100, (240). The unit-cell parameters, obtained by refinement of the X-ray powder data accepting that the mineral is triclinic, crystallizing in space group $P1$, are $a = 7.699(3)$ Å, $b = 12.220(7)$ Å, $c = 6.702(2)$ Å, $V = 583.1(9)$ Å³; $\alpha = 93.97(1)^\circ$, $\beta = 93.07(2)^\circ$, $\gamma = 68.20(1)^\circ$.



Figure 16. Rhodonite (pink), calcite (white, top), sphalerite (small, black), and sudoite (gray green) (left); banded from bottom to up: quartz, rhodonite, calcite, quartz, calcite + sphalerite, calcite and quartz crystals (right). Photographs by Ana Tudor.

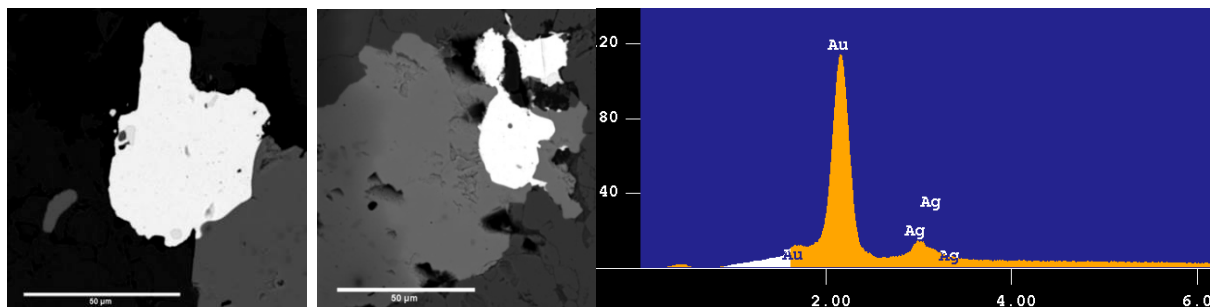


Figure 17. Backscattered electron image of gold (white, large isometric grains), manganian ilvaite (dark gray), sphalerite (gray), and quartz (black) - (left) and its simplified electron diffraction spectrum (right). (Hirtopanu et al., 2012).

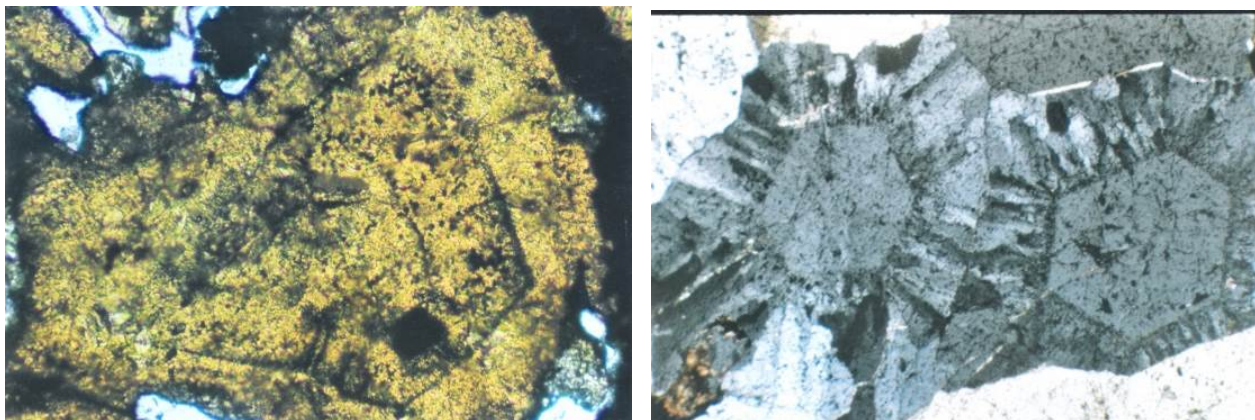


Figure 18. Zoned sphalerite. Transmitted light, NII, x30 (left). Zoned quartz: idiomorphic hexagonal crystal (center) with peripheral fibrous aggregates (right). Transmitted light, N+, x20 (right).

No relations between rhodonite and manganian ilvaite can be established. As regarding hubeite, rhodonite seems to belong to other high-temperature stage than this one, which seems formed in an earlier stage of evolution, most probably at higher temperature.

4. OTHER ASSOCIATED MINERALS

4.1. Native gold

The gold from Cavnic closely associates with manganian ilvaite, pyrite, and sphalerite. The grains of native gold have an isometric shape (Figure 17 left) dimensions varying between few microns and 1 mm. The mineral can be easily seen on optical microscope. In the backscattered electron images one can see many grains of native Au forming little veins on the fine cracks of the manganian ilvaite (Figure 15 left).

Native gold also surrounds pyrite grains (Figure 15, left). The textural relations depicted before suggest that the native gold formed later as compared with manganian ilvaite and pyrite. The electron diffraction spectrum of native gold (Figure 17, right) shows low contents of silver (about 2 wt.%) in solid solution.

The main lines in the powder diffraction pattern, expressed in terms of d spacings (in Å), relative intensities (I/I_0 , %) and Miller indices (hkl) are: 2.35, 100, (111); 2.03, 75, (200); 1.44, 75, (220); 1.23, 88, (311); 1.17, 62, (222). The unit-cell parameters, refined on the basis of the X-ray powder data, accepting the crystallization in the space group $Fm-3m$ (225) is $a = 4.068(1)$ Å, $V = 67.32(1)$ Å³.

4.2. Sphalerite

Sphalerite, ideally (Zn,Fe)S, has a yellow color in transmitted light and is frequently zoned (Figure 18, left). The unit-cell parameters refined on the basis of X-ray powder data are: $a = 5.437(1)$ Å, $V = 160.72(2)$ Å³.

4.3. Pyrite

Pyrite (FeS₂) occurs on the cracks of manganian ilvaite and is associated with native gold (Figure 15 left). The gold grains surround the pyrite crystals. They could have the same low forming temperature as pyrite. All sulfides crystallized after sudoite, most probably at $T = 180 - 200^\circ\text{C}$ (Piantone et al., 1999).

4.4. Quartz

Quartz has two growth phases, as follows: the

first phase has a hexagonal idiomorphic shape, on which grows radiating aggregates of fibrous quartz pertaining to the second phase (Figure 18 right).

5. CONCLUSIONS

The finding of hubeite at Cavnic marks the first occurrence of this mineral in Romania and the third occurrence in the world. The X-ray powder data recorded for this mineral, as well as the unit-cell parameters, fit well with those of the type material from Hubei Province, China. Hubeite occurs closely associated with inesite, also found for the first time in Romania. Reciprocal textural relations show that inesite is older than hubeite. Inesite is iron-free and occurs in relatively reducing conditions, whereas hubeite, which contains Fe³⁺ in its composition, occurs in moderate oxidizing conditions.

Ruizite, also mentioned for the first time in Romania at Cavnic by this work, is also an iron-free Ca-Mn hydrated silicate, containing Mn³⁺ in its composition, which indicates the crystallization at high oxygen fugacities. It occurs in close association with manganian ilvaite. Both hubeite and ruizite are Ca-Mn hydrated silicates. However, all Mn is divalent in hubeite and trivalent in ruizite. In addition, ruizite is Fe-free, whereas hubeite contains significant Fe³⁺. Ruizite was formed under higher oxidizing conditions than hubeite. It is associated with apophyllite, sudoite, manganian ilvaite, specularite, quartz, and sphalerite.

The Cavnic manganian ilvaite has not relics of the early-skarn Mn-pyroxenes (hedenbergite - johannsenite) and Mn-pyroxenoids (rhodonite or bustamite). The textural relations show that inesite, hubeite, and ruizite are most formed on the expense of manganian ilvaite, in the low T hydrothermal environment.

Manganian ilvaite of the inesite + hubeite/ + ruizite + apophyllite + sudoite assemblage seems to be a direct product of the hydrothermal process in a medium oxidizing and hydrous environment, being the oldest mineral in this assemblage. Also, its low Mn content could indicate a hydrothermal origin.

The carbonate associated with the ruizite + manganian ilvaite + sudoite + specularite association is a calcian-manganian siderite, and not a rhodochrosite or calcite. The last one is associated to rhodonite in the higher T assemblage, in other place of deposit.

The native gold is closely related to the association manganian ilvaite / pyrite / galena / sphalerite, and crystallized during the latest stage of the hydrothermal evolution of the system, most probably at $T = 180 - 200^\circ\text{C}$.

The fluid inclusion study (Piantone et al., 1999) reveals a global cooling of the Cavnic ore-system from 320°C to 200°C. Crystallization temperatures calculated for the sphalerite/galena assemblage of stage 3 range between 234 and 290°C (Piantone et al., 1999), indicative for an epithermal deposit. The inesite + hubeite + ruizite + apophyllite + sudoite + siderite assemblage crystallizes later, belonging to the early epithermal stage (200°C), whereas the gold mineralization could be considered as late epithermal.

REFERENCES

- Appleman, D.E. & Evans, H.T., Jr.**, 1973. *Indexing and least-squares refinement of powder diffraction data*. U.S. Geol. Surv., Comput. Contrib. 20 (NTIS Doc. PB-216).
- Balestra, C., Kolitsch, U., Blass, G., Callegari, A.M., Boiocchi, M., Armellino, G., Ciriotti, M.E., Ambrino, P. & Bracco, R.**, 2009. Mineralogia figure 2007-2008: novità caratterizzate dal Servizio UK dell'AMI. Micro. 1-2009. *Ruizite*. 78-99.
- Benoit, P.H.**, 1987. *Adaptation to microcomputer of the Appleman-Evans program for indexing and least-squares refinement of powder-diffraction data for unit-cell dimensions*. Am. Mineral. 72, 1018-1019.
- Borcoş, M., Lang, B., Boştinescu, S. & Gheorghişă, I.**, 1975. *Neogene hydrothermal ore deposits in the volcanic Gutâi Mountains*. Part III. *Révue Roumaine de Géologie, Géophysique et Géographie, Série Géologie*, 19. 21-35.
- Bonev, I.K., Vassileva, R.D., Zotov, N. & Kouzmanov K.**, 2005. *Manganilvaite, $CaFe^{2+}Fe^{3+}(Mn,Fe)(Si_2O_7)(O)(OH)$, a new mineral of the ilvaite group from Pb-Zn skarn deposits in the Rhodope Mountains, Bulgaria*. Can. Mineral., 43 (3), 1027-1042.
- Colville, A.A., Anderson, C.P. & Black P.M.**, 1971. *Refinement of the crystal structure of apophyllite. I. X-ray diffraction and physical properties*. Am. Mineral., 56, 1222-1233.
- Cooper M. A. & Howthrow F. C.**, 2002. *The crystal structure of hubeite $Ca_2Mn^{2+}Fe^{3+}[Si_4O_{12}OH](H_2O)_2$, a novel sorosilicate mineral*. Can. Mineral., 42, 825-834.
- Eggleston, R.A. & Bailey, S.W.**, 1967. *Structural aspects of dioctahedral chlorite*. Am. Mineral., 52, 673-689.
- Fendrich, K.V., Downs, R.T. & Orglieri, M.J.**, 2016. *Redetermination of ruizite, $Ca_2Mn^{3+}_2[Si_4O_{11}(OH)_2](OH)_2H_2O$* . Acta Cryst., E72, 959-963.
- Hîrtopan, P., Andersen, J.C., Hîrtopan I. & Udubaşa, S.S.**, 2012. *Ilvaite from the Cavnic deposit, Romania*. Romanian Journal of English Studies, 62-65.
- Holtstam, D.**, 2020. *Hubeite from Haristigen mine*. Journal Langbansnytt, 26,13-14.
- Howthorne, F.C.**, 1984. *The crystal structure of ruizite, a sorosilicate with an $[Si_4O_{13}]$ cluster*. Tschermarks mineralogische und petrographische Mitteilungen, 33 (2), 135-146.
- Howthorne, F.C., Cooper, M.A., Grice, J.D., Roberts, C.A., Cook, W.R. & Lauf, R.J.**, 2002. *Hubeite, a new mineral from the Daye mine near Huangshi, Hubei Province, China*. Mineralogical Record, 465-471.
- Ilinca, G., Vizitiu, A., Topa, D. & Vlad, Ş.**, 2006. *A new occurrence of manganilvaite at Dognecea, Southwestern Banat, Romania: chemical composition, crystal structure, and cation ordering*. Acta Mineralogica-Petrographica, Abstract Series, Szeged, 5, 1-47.
- Jige, M., Kitagawa, R., Zaykov, V.V. & Sinyakov, I.**, 2018. *Surface microtopography of sudoite*. Clay Minerals, 38 (3), 375-382.
- Jude, R.**, 1986. *Metalogeneza asociată vulcanismului neogen din NV Munţilor Oaş*. Ed.Acad. Rom., 0-132.
- Larsen, A.O. & Dahlgren, S.**, 2002. *Ilvaite from the Oslo Graben, Norway*. Neues Jahrbich fur Mineralogie, Monatshefte, 4, 169-181.
- Lang, B., Edelestein, O., Steinitz, G., Kovacs, M. & Halga, S.**, 1994. *Ar-Ar dating of adularia - a tool in understanding genetic relations between volcanism and mineralization: Baia Mare area (Gutâi Mountains), Northwestern Romania*. Ec. Geology, 89 (1), 174-180.
- Momoi, H.**, 1974. *Hydrothermal crystallization of $MnSiO_3$ polymorphs*. Min. Journ., 7, 359-373.
- Moore, P., B, Shen, J. & Araki, T.**, 1985. *Crystal chemistry of the $(M2)_{3+}$ phi2 sheet: Structural principles and crystal structures of ruizite, macfallite and orientate*. Am. Mineral., 70, 171- 81.
- Piantone, P., Bailly, L., Nehlig, P., Grancea, L., Leroy, J., Marias, Z. & Marcoux, E.**, 1999. *Fluid inclusion and isotope study of the Cavnic epithermal deposit, Romania*. Mineral Deposits: Processes to Processing. Stanley et al. (eds). Volume 1, 79-82.
- Plimer, I.R. & Ashley, P.M.**, 1978. *Manganoan ilvaite from Broken Hill, N.S.W., and Ban Ban, Queensland Australia*. Mineral. Mag., 42, 85-88.
- Kearns, L.E. & Kearns, C.A.**, 2008. *Ruizite in Cornwall Iron Mine, Pennsylvania, Lebanon County*, Mineral News, 24, 8-9.
- Williams, S.A. & Duggan M.**, 1977. *Ruizite, a new silicate mineral from Christmas, Arizona*, Mineral. Mag., 41, 429-432.
- Wilson, W.E. & Dunn, P.J.**, 1978. *The Kalahari manganese field*, Mineral. Record, 9, 137-153.

Received at: 23. 02. 2022

Revised at: 03. 08. 2022

Accepted for publication at: 08. 08. 2022

Published online at: 17. 08. 2022